Modeling of Dynamic Effects Caused by the Beam Delivery System in Selective Laser Sintering

Irem Y. Tumer, Graduate Research Asst.
Kristin L. Wood, Associate Professor
Ilene J. Busch-Vishniac, Professor

Mechanical Engineering Department
The University of Texas at Austin

Abstract

In this work, the machine dynamic response in Selective Laser Sintering is investigated with the purpose of determining the causes of scanning errors. Machine subcomponents are first investigated to determine their potential effects on the laser beam positional accuracy. The dynamics of the laser beam delivery system are identified as the major contributor to deviations in the laser beam position. The moving-iron galvanometer scanner used in SLS machines is then modeled, with the ultimate goal of understanding how its various components and parameters affect part scanning accuracy. This work should provide a better understanding of the dynamics of the laser beam delivery system and give insight on machine parameters that result in better part accuracy.

1 Introduction

The machine dynamic response in Selective Laser Sintering (SLS) is investigated in order to identify the sources of deviations in the laser beam positioning accuracy. The results of this work will be used to determine diagnostic and corrective measures to produce parts with improved accuracy and precision. In this paper, the different SLS machine modes are investigated to determine which machine components affect part accuracy and precision.

This work focuses on investigating the machine components that result in deviations in the scanning process, which in turn affect the accuracy of finished SLS parts. Scanning errors result when the laser beam position deviates from its ideal scan path. Note that any vibrations in the system's machine components can presumably cause the laser beam delivery system to vibrate excessively. These deviations in the laser beam position will manifest as spatial errors on the finished parts. Once we determine which machine components result in scanning errors, we can then investigate subsystems to determine how various parameters affect part scanning.

2 SLS Machine Response: Modeling and Simulation

The purpose of the overall project is to control part accuracy of parts produced by the Selective Laser Sintering process. The main physical phenomena that are being investigated include the machine dynamic response and the in-bed thermal and material response [12]. The current focus of this portion of the project is on studying part accuracy with respect to the machine dynamic response only. The following work presents the development of a physical model of the machine response in order to determine the resulting dynamic machine modes.

2.1 A Study of the System Machine Components

A schematic of the machine components that will potentially affect the laser beam position is provided in Figure 1. As shown in the figure, the major moving machine subsystems that might cause a deviation in the laser beam position are the roller system, the part and powder cylinders, and the scanner system. The main question to be answered is whether any of these components will cause dynamic modes that will result in deviations from the ideal part shape and dimensions

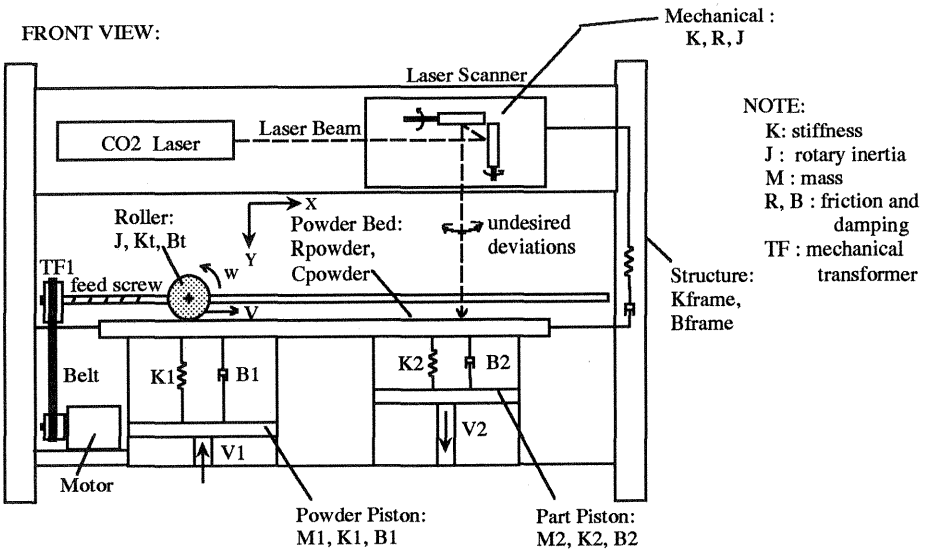

Figure 1: SLS Machine Elements.

scanned on the powder surface. A simple approach to investigate this issue is to create lumped-parameter models of the machine subsystems, and compute settling times to determine whether the oscillations will damp out by the time the laser starts scanning.

The powder leveling system, one of the major moving subsystems of the machine, is investigated first. Prior to laser scanning, the roller travels over the powder to evenly deposit a thin layer of powder on the bed. Once the laser returns to its starting position and stops rotating, laser scanning begins. Any transmitted vibrations caused by the dynamics of the roller system will affect the positional accuracy of the laser beam. Note that, the roller translates along the powder bed by means of a feed screw, while providing a counter-rotating motion to evenly spread the powder. As a result, both the translational and rotational motions need to be studied individually.

The rotational motion of the powder leveling system is modeled as shown in Figure 2a. A second-order model of this system is also provided in Figure 2a, as well as the model parameters. Note that the inertia and stiffness components will contribute to the natural frequency of the system, while the damping will determine how quickly the vibrations will settle to a steady state. The translational motion of the powder leveling system is modeled as shown in Figure 2b, along with a second-order model, and the model parameters.

A set of performance measures can be used to characterize the response of these second-order systems. This set of quantitative specifications is commonly used to describe the response of any second-order system, without the need to sketch the response [9]. For example, for the rotational roller motion, the natural frequency of the second-order system, $\omega_n = \sqrt{\frac{K_t}{J_t}}$, is the frequency of oscillation of the system without damping. The damping ratio, $\zeta = \frac{B_t}{2J_t\omega_n}$, determines the nature of the response, from underdamped to a completely oscillatory response. The settling time, $T_s = \frac{4}{\zeta\omega_n}$, determines the amount of time required for the transient response's damped oscillations to reach 2% of the steady-state value. The model parameters (J_t, K_t, and B_t) are computed from the geometry and material properties of the subsystems.

These measures are presented for both subsystems in Table 1. Note that, the translational cycle of the roller before the laser starts scanning the powder bed is about 20 *seconds*. In addition to the result from the model, vibrations of the roller measured using an accelerometer show that, once the roller stops moving, all oscillations due to the roller dynamics damp out within 1 *second*. Laser scanning begins several seconds after the roller stops moving. As a result, we conclude that the

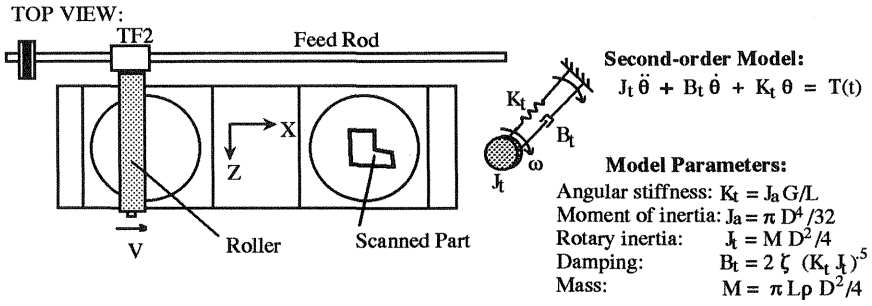

(a) Rotational System.

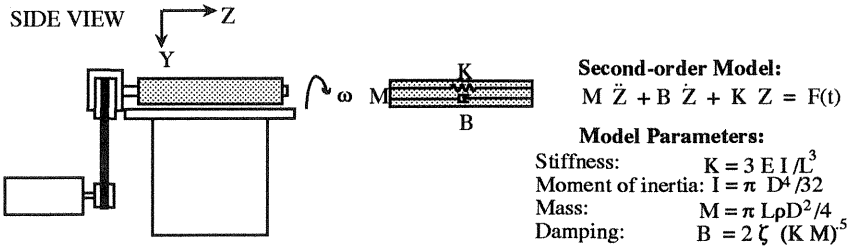

(b) Translational System.

Figure 2: Roller subsystem models.

Performance Measure	Roller Subsystem (Rotational Motion)	Roller Subsystem (Translational Motion)
Natural Frequency (rad/sec)	5134	646
Damping Ratio	0.005	0.0075
Settling Time (sec)	0.156	0.825

Table 1: Performance Measures for Subsystem Models.

oscillations due to the roller motion will have damped out by the time the laser starts scanning the part.

Another subsystem consists of the part and powder cylinders, which move by fixed amounts to deliver a new layer of powder before each scanning session begins. Vibrations measured using an accelerometer show that the oscillations caused by this motion on the top plate of the pistons will damp out within 0.5 *seconds*. Since the piston motion precedes the roller motion, any vibrations caused by the piston motion will have settled by the time laser scanning begins; hence, these subsystems are eliminated as candidates causing positional deviations of the laser beam. Finally, damping mechanisms are implemented throughout the SLS machine to prevent the frame structure from transferring any vibrations that might result from external as well as internal sources. Oscillations of the frame structure measured with an accelerometer at several different locations show no significant vibrations due to external sources; in addition, oscillations caused by an impact on the frame structure damp out in less than 200 *ms*. These initial findings are confirmed by Desktop Manufacturing, Inc. in internal studies done on accuracy and vibrational modes of the machine [3, 4].

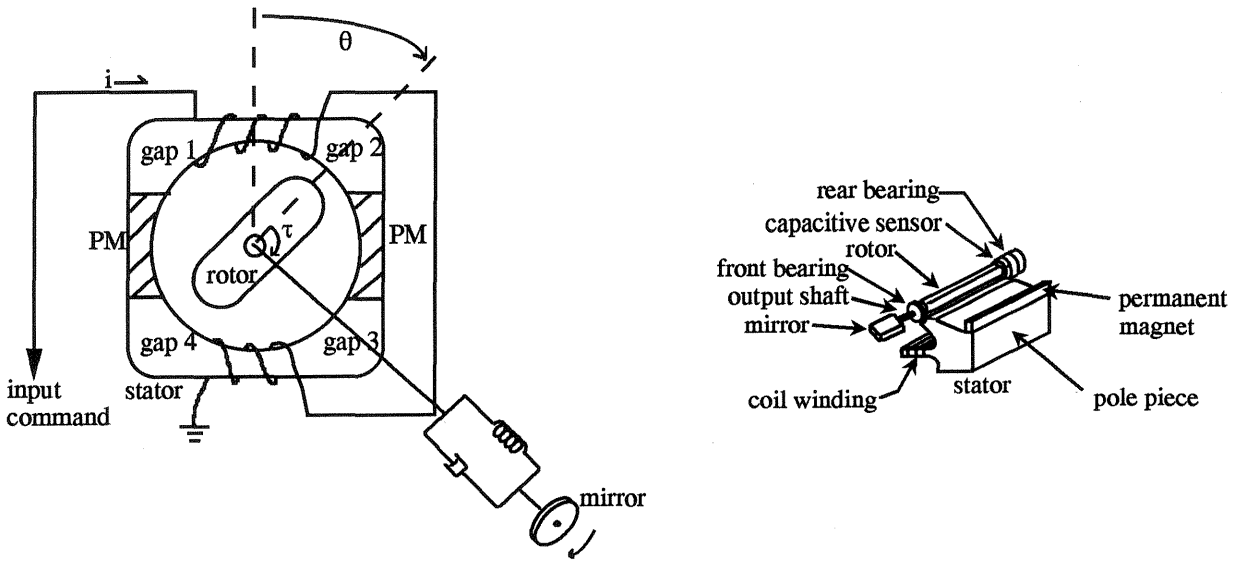

(a) Internal Components. (b) Cut-away View.

Figure 3: Moving-Iron Galvanometer.

2.2 The Scanner System

The preliminary studies of the SLS machine response identify the scanners as the only candidate machine component contributing to surface errors. In SLS, two scanners are used to direct the laser beam by means of two orthogonally-placed mirrors. The lower scanner has a smaller mirror and produces the X scan. The upper scanner has a larger mirror that reflects the X axis in the Y direction, producing the Y scan [11]. The scanner heads use low-inertia galvanometers, used as a servo-driver with low external loads, actuated by means of a moving coil or moving iron [6, 13]. Figure 3a shows a moving-iron type of galvanometer, developed by General Scanning, Inc. [11], currently used in the SLS machines [6]. Figure 3b shows a detailed cut-away view of a moving-iron galvanometer.

2.2.1 Physics of the Galvanometers

The General Scanning moving-iron type of galvanometers [11] derive their mechanical torque from the interaction of an electromagnetic circuit provided by the drive coils, and the magnetic field of a permanent magnet [6]. The device is designed to provide a limited rotation angle between minimum and maximum flux locations in the field. Because of the symmetry of the device, gaps 1 & 3 and gaps 2 & 4 have identical energy conditions. In addition, since the permanent magnets have permeability comparable to air, poles 1 & 2 are disassociated from poles 3 & 4 (see Figure 3a). As a result, energy can be assessed for gaps 1 and 2 and multiplied by two to obtain the total energy. Furthermore, because the electromagnetic fields are linear, superposition can be used to compute energy in gaps as the sum of the values of all independent fields; hence, each air gap supports the sum of the fields generated by the permanent magnets plus the field induced by the drive coil, which can be derived independently. Finally, when the drive coils are not powered, the air gaps support the component of the magnetic field generated by the permanent magnets only, which is assumed independent of the rotor angular position based on geometry.

Because of the geometry of the galvanometers, the rotor will move between two positions, in the direction dictated by the current in the coils. When a positive current is put in through the coils,

gap 1 will have a magnetic flux due to the permanent magnet plus a flux due to the electromagnet from the drive coils, entering through the gap between pole 1 and the rotor. Gap 2 will have a flux generated by the permanent magnet on the right side minus the flux generated by the drive coils in the effective gap area between pole 2 and the rotor. Hence, the rotor will move from a position of symmetry to a position of minimum reluctance. This angular motion is controlled by the magnitude and direction of the current in the drive coils.

Based on these assumptions and observations, the total energy in the magnetic system is provided by the sum of the individual energy terms in gap 1 and gap 2, multiplied by 2 to account for the symmetry of the remaining two poles, as shown in Equation 1:

$$E(\theta, \varphi) = \frac{g}{\mu_0}\left(\frac{\varphi_1^2}{A_1} + \frac{\varphi_2^2}{A_2}\right) \tag{1}$$

where φ_1 and φ_2 are the total flux values in gaps 1 and 2 respectively, and include the flux generated from the permanent magnets and the coil; A_1 and A_2 are the effective magnetic field areas for the two gaps; μ_0 is the permeability of air; and g is the air gap size. The torque generated by the magnetic system is computed by taking the partial of total energy with respect to angle of rotation, θ. Similarly, the magnetomotive force generated by the system is the partial of total energy with respect to coil flux. We substitute for $\varphi_1 = \varphi_{coil} + B_{PM}A_1$, $\varphi_2 = -\varphi_{coil} + B_{PM}A_2$, $A_1 = rL(\alpha - \theta)$, and $A_2 = rL(\alpha + \theta)$, where B_{PM} is the constant magnetic field generated by the permanent magnets, φ_{coil} is the flux generated by the coils, α is the overlap angle between the pole and the rotor, θ is the angle of rotation of the rotor, r is the radius of the rotor and, L is the axial length of the rotor piece. The resulting torque and magnetomotive force expressions are provided in Equation 2:

$$\begin{aligned} \tau &= \frac{4g\alpha\theta\varphi_{coil}^2}{\mu_0 rL(\alpha^2 - \theta^2)^2} + \frac{4gB_{PM}\alpha\varphi_{coil}}{\mu_0(\alpha^2 - \theta^2)} \\ \Delta M &= \frac{4g\alpha\varphi_{coil}}{\mu_0 rL(\alpha^2 - \theta^2)} \end{aligned} \tag{2}$$

2.2.2 Simple Scanner Model

Scanner systems have been modeled in the literature to determine their general response characteristics, their accuracy, and repeatability [1, 2, 8, 13]. These are typically simple models used to determine the general behavior of scanners. The models are used in conjunction with controller models to determine the best control to assure scanner accuracy and repeatability. Such a simple second-order model of the scanner is shown in Figure 4. A simple second-order model of the scan-

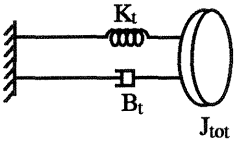

Second-order Model:

$J_{tot}\ddot{\theta} + B_t\dot{\theta} + K_t\theta = KI$

Model parameters:

J_{tot}: mirror & rotor inertia
B_t : damping
K_t : angular stiffness
K : torque constant
I : input current
θ : angular position

Figure 4: Simple Galvanometer Model.

ner system and a description of the model parameters are also provided in Figure 4. The rotary inertias, angular stiffness, and torque constant are provided in Appendix A, whereas the remaining can be computed based on the dimensions and material properties of the scanner components.

The response based on this simple model is presented in Figure 5. As expected from the physics

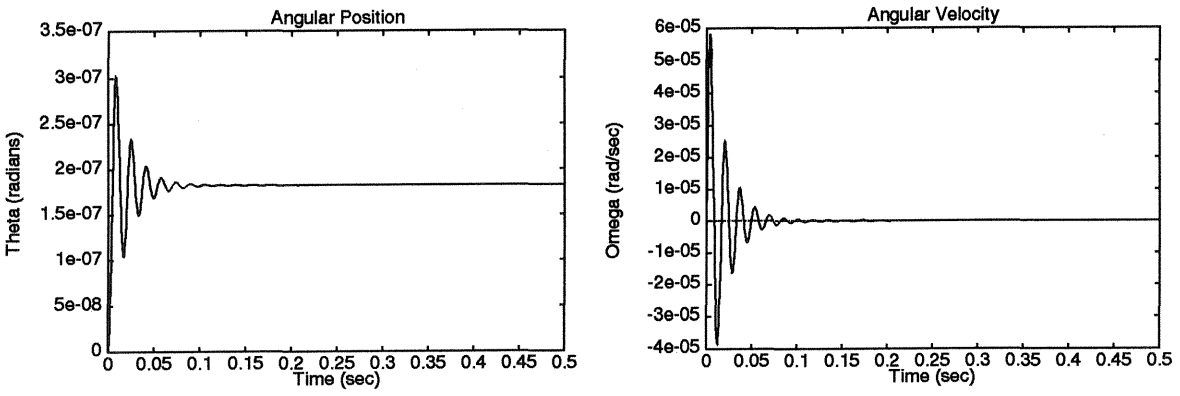

Figure 5: Simulation Results: a) Mirror Angular Position, and, b)Angular Velocity.

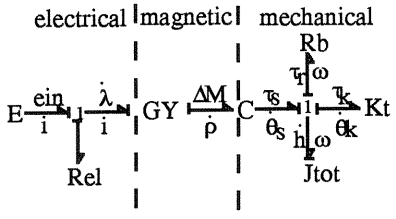

Bond-graph elements:

E : voltage source
Rel : electrical resistance
GY : gyrator (motor)
C : multi-port capacitance (magnetic & mechanical)
Rb : bearing & internal damping
Kt : angular stiffness

Power variables:

ein: input voltage
i : coil current
λ : flux linkage
ΔM : magnetomotive force
ρ : magnetic flux
τ : mechanical torque
θ : angular position
ω : angular velocity
h : angular momentum

Figure 6: Bond Graph Model of the Galvanometer System.

of the galvanometer system, given a constant input, the angular position of the mirror settles to a constant value, where the rotor stops moving and hence the velocity settles to zero. Based on this model, we can show that the choice of the design parameters becomes very important in obtaining an acceptable response. For example, increasing the mirror and rotor inertias or increasing the stiffness of the mirror shaft results in an increasing oscillatory response, which in turn will result in beam positional deviations when scanning a part on the powder bed. Reduced damping has a similar effect since the response will take longer to settle. Inertia, damping, and stiffness are determined by the choice of design parameters in the scanner system. Using models such as the one presented here, the designers can predict the response based on the choices they make.

2.2.3 Detailed Bond-Graph Model

Unfortunately, simple scanner models do not provide a complete picture of the physical phenomena resulting in the angular movement of the scanner mirrors. In actual devices, perturbations exist as a result of the nonlinearities of the torque versus rotor angle and of the torque versus current. In addition, the inductance (or reluctance) presented to the amplifier is position dependent. These phenomena lead to the need for a more detailed model for the galvanometer system.

A detailed model is developed using bond graph modeling techniques, and is shown in Figure 6. The model is based on the cut-away view (Figure 3b) and the detailed view of the electromagnetic circuitry driving the system (Figure 3a), and derived using common electromagnetic actuator models [5, 7, 10]. Note that this is a fourth-order model, where the state variables corresponding to energy-storing components are, φ (magnetic flux), θ (total angular position), h (angular momentum), and θ_k (shaft angular oscillations). The magnetic compliance effort variables, τ_s and

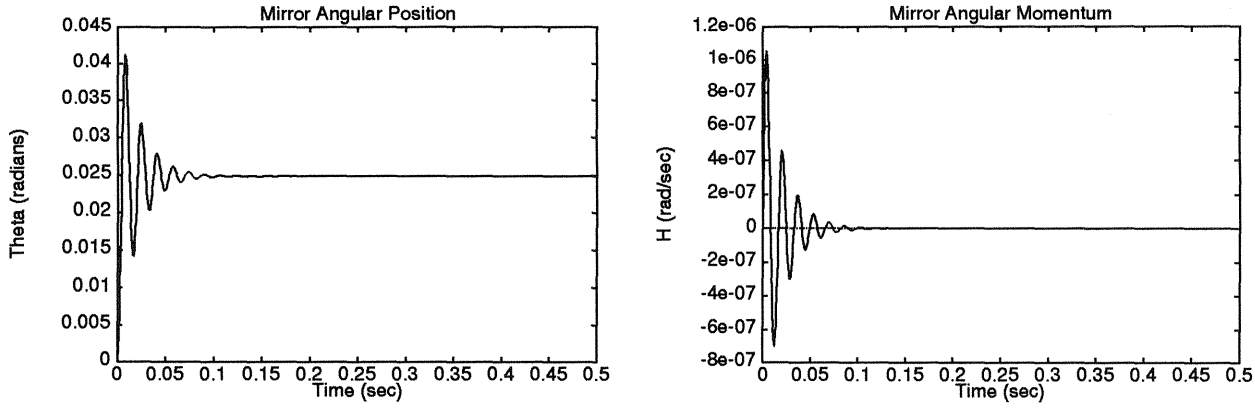

(a) Angular Position.

(b) Angular Momentum.

Figure 7: Preliminary Simulation Results from the Bond-Graph Model.

ΔM, are derived based on the moving-iron circuitry, which converts the electromagnetic input into a rotary motion of the rotor, supplying the necessary torque to drive the output shaft connected to the mirror. Typically, this type of device is modeled by computing the energy stored in the system [5, 6]. The total energy, magnetic torque τ, and the magnetomotive force ΔM are shown in Equations 1 and 2. Finally, the damping due to the bearings is derived assuming that a viscous bearing friction torque is generated at the rotor.

The set of first-order simultaneous differential equations derived from the bond graph model completely describes the response of the system. The state equations, as well as the model and system parameters are presented in Appendix A. Based on these equations, the preliminary simulation results are presented in Figure 7.

As can be seen from the plots, the bond-graph model results follow the general shape of the results from the simple second-order model (see Figure 5); the angular position settles to a constant value, whereas the angular momentum settles to zero. As in the case of the simpler model, increasing the stiffness of the shaft results in an increased oscillatory response with smaller amplitudes, with no change in the settling times. Increasing the rotary inertia values results in an increased oscillatory response, as well as a longer settling time. Finally, decreasing damping in the model results in an increased oscillatory response, with a very high settling time. However, using the bond-graph model, even though the settling times are the same as in the case of the simpler model results, the amplitudes of the vibrations are much greater. The difference between the two simulation results are currently being investigated.

2.3 Planned Study of SLS Machine Response

The results of the bond-graph model will be used to better understand the laser beam positional deviations with respect to scanner parameters. Given the set of parameters that can be controlled and the complete and accurate analytical model, we first need to determine what accuracy levels are acceptable. The first measure of performance is based on simulation results, performing a visual comparison with respect to system parameters. Other measures could be typical measures to quantify dynamic systems, such as time constants, settling times, percent overshoot, etc. A thorough analysis of the model output with respect to the system parameters should identify the ranges of parameters for best accuracy, as well as the components that might cause errors due to their dynamics (such as compliances, inertia, and resistances from each component). Other mathematical measures will be developed to better quantify the composite error in the response

signal generated by the model, and a similar study will be performed to study deviations of the laser beam position.

2.4 Supporting Experimentation

Several experiments are currently being designed. The simplest experiment consists of using mylar sheets or photographic paper to scan simple forms and measure the scanning errors using a scaled microscope. Similar experiments will determine the precision (repeatability) of the scanners by moving the laser beam to the same target position at different times, and measuring the positional deviations from the target position. The variance of these measurements will provide a measure of the precision (repeatability) of the laser beam position.

A more thorough experimental set-up will consist of a diode laser, galvanometer scanners, and a photodetector to measure the scanning position digitally. The photodetector will be connected to a data acquisition system to record the signal from the scanner motion. Results from these experiments will determine the accuracy of the laser beam positional measurement. Signals measured by the photodetector will be used to determine the nature of the possible temporal modes resulting from the machine dynamics.

3 Conclusions

This paper presents physical models of the machine dynamic response of the Selective Laser Sintering system. The galvanometric scanners are identified as the major contributor to the laser beam positional deviations while scanning a part. A preliminary model of the galvanometers is developed. The model results will be used to obtain a better understanding of how the scanner design parameters affect the accuracy of finished SLS parts. The results will also be used to identify specific machine modes and provide corrective measures to improve part accuracy in Selective Laser Sintering. Experiments are proposed to further investigate the SLS system parameters that affect part accuracy.

4 Acknowledgements

This material is based on work supported, in part, by The National Science Foundation, Grant No. DDM-9111372; an NSF Presidential Young Investigator Award; by a research grant from TARP; plus research grants from Ford Motor Company, Texas Instruments, and Desktop Manufacturing Inc., and the June and Gene Gillis Endowed Faculty Fellowship in Manufacturing. Any opinions, findings, conclusions or recommendations expressed in this publication are those of the authors and do not necessarily reflect the views of the sponsors.

References

[1] P. Brossens. Scanning accuracy of the moving-iron galvanometer scanner. *Optical Engineering*, 15:2:95–98, March/April 1976.

[2] A. Bukys. Considerations in the design of servo amplifiers for high performance scanning systems. *SPIE Proceedings: Beam Deflection and Scanning Technologies*, 1454:186–195, 1991.

[3] Paul Forderhase. "Part Accuracy DOE Studies ". Personal conversation about DOE studies on dimensional accuracy, October 1994.

[4] Product Genesis. Laser table vibration and thermal analysis summary. *Confidential Internal Document*, October 1991.

[5] D. Karnopp. Bond graph models for electromagnetic actuators. *Journal of the Franklin Institute*, 319,1/2:173–181, January/February 1985.

[6] G.F. Marshall. *Laser Beam Scanning.* Marcel Dekker, Inc., New York, 1985.

[7] L.W. Matsch and J.D. Morgan. *Electromagnetic and Electromechanical Machines.* Harper and Row, Publishers, New York, 1986.

[8] J. Montagu. A practical approach to low inertia scanner selection. *SPIE Proceedings: Laser Components and Techniques*, 84:42–46, August 1976.

[9] N.S. Nise. *Control Systems Engineering.* The Benjamin/Cummings Publishing Company, Inc., Redwood City, Ca, 1991.

[10] D.V. Richardson and A.J. Caisse. *Rotating Electric Machinery and Transformer Technology.* Prentice Hall, Inc., Englewood Cliffs, New Jersey, 1987.

[11] General Scanning. *X-Y Scan Head Series User Manual.* Watertown, Massachusets, 1986.

[12] K.L. Wood and T. Bergman. Precision and repeatability in polymeric sls. *Research Proposal to the Advanced Technology Program*, June 1993.

[13] Y.-J. Wu. *Minimum Time Laser Tracking Control Technique for Selective Laser Sintering.* PhD thesis, The University of Texas, Austin, Tx, 1992.

A State Differential Equations from Bond Graph Model

$$\begin{aligned}
\dot{\varphi} &= \frac{1}{N}E_{in} - \frac{R_{el}}{N^2}\Delta M \\
\dot{\theta} &= \frac{h}{Jtot} \\
\dot{h} &= \tau_s - K_t\theta_k - \frac{B_{tot}}{J_{tot}}h \\
\dot{\theta_k} &= \frac{1}{J_{tot}}h
\end{aligned}$$

where φ is the coil flux, θ is the angle of rotation, h is the angular momentum, θ_k is the shaft angular oscillations. The values for τ_s and ΔM are given in Equation 2. J_{tot} is the sum of the rotor and mirror inertias. B_{tot} is the sum of estimated viscous damping from the bearings and the shaft internal damping. The remaining parameters from General Scanning [11] (for scanner model G120DT and mirror model G300, 10 mm) and the estimated parameters are given in Table 2.

Constant	Description	Provided Value	Estimated Value
N	Number of coil turns	175 *turns*	
α	Overlap angle		0.002 *rad*
E_{in}	Input voltage		2 *Volts*
g	Air gap size	10^{-4} *m*	
μ_0	Permeability of air	$4\ \pi\ 10^{-7}$ *H/m*	
D_r	Rotor diameter	$4.6\ 10^{-3}$ *m*	
L_r	Rotor axial length	$33\ 10^{-3}$ *m*	
J_r	Rotor rotary inertia	$0.028\ 10^{-7}$ *kg m*^{2}	
J_m	Mirror rotary inertia	$1.3\ 10^{-7}$ *kg m*^{2}	
K_t	Angular Stiffness	0.02 *kg m*^{2}	
B_s	Internal Shaft Damping		$3.0\ 10^{-6}$ *Nmsec/rad*
R_b	Bearing Damping		$1.1\ 10^{-5}$ *Nmsec/rad*
R_{el}	Coil Resistance	2.0 Ω	
L_{el}	Coil Inductance	1 m*H*	
K	Torque constant	0.011 *N m/A*	
B	Constant PM field	1 *T*	

Table 2: Constants for the Bond Graph Model.